Gap junctions on hippocampal mossy fiber axons demonstrated by thin-section electron microscopy and freeze–fracture replica immunogold labeling

Farid Hamzei-Sichani*†, Naomi Kamasawa‡§, William G. M. Janssen¶, Thomas Yasumura‡, Kimberly G. V. Davidson‡, Patrick R. Hof¶‖, Susan L. Wearne¶‖, Mark G. Stewart, Steven R. Young**, Miles A. Whittington††, John E. Rash‡,‡‡, and Roger D. Traub****

*Program in Neural and Behavioral Science, **Department of Physiology and Pharmacology, State University of New York, Downstate Medical Center, 450 Clarkson Avenue, Brooklyn, NY 11203; ‡Department of Biomedical Sciences, ‡‡Program in Molecular, Cellular, and Integrative Neurosciences, Colorado State University, Fort Collins, CO 80523; ¶Department of Neuroscience, ‖Computational Neurobiology and Imaging Center, Mount Sinai School of Medicine, New York, NY 10029; and ††School of Neurology, Neurobiology, and Psychiatry, The Medical School, University of Newcastle, Newcastle NE1 7RU, United Kingdom

Communicated by Nancy J. Kopell, Boston University, Boston, MA, June 13, 2007 (received for review May 1, 2007)

Gap junctions have been postulated to exist between the axons of excitatory cortical neurons based on electrophysiological, modeling, and dye-coupling data. Here, we provide ultrastructural evidence for axoaxonic gap junctions in dentate granule cells. Using combined confocal laser scanning microscopy, thin-section transmission electron microscopy, and grid-mapped freeze–fracture replica immunogold labeling, 10 close appositions revealing axoaxonic gap junctions (≈30–70 nm in diameter) were found between pairs of mossy fiber axons (≈100–200 nm in diameter) in the stratum lucidum of the CA3b field of the rat ventral hippocampus, and one axonal gap junction (≈100 connexons) was found on a mossy fiber axon in the CA3c field of the rat dorsal hippocampus. Immunogold labeling with two sizes of gold beads revealed that connexin36 was present in that axonal gap junction. These ultrastructural data support computer modeling and *in vitro* electrophysiological data suggesting that axoaxonic gap junctions play an important role in the generation of very fast (>70 Hz) network oscillations and in the hypersynchronous electrical activity of epilepsy.

axoaxonic | connexin | electrical synapse | epilepsy | synchronization

Granule cells in the hippocampal dentate gyrus provide a major source of synaptic excitation to CA3 pyramidal neurons via morphologically complex mossy fiber (MF) terminals that wrap around large spines (thorny excrescences) on the proximal segment of apical dendrites of the postsynaptic neurons (1). Individual granule cells *in vivo* have low spontaneous firing rates (2), yet they exert powerful effects when they fire a burst of action potentials, causing the discharge of postsynaptic CA3 pyramidal neurons (1, 3). Gap junctions between axons of cortical excitatory (principal) neurons were predicted to exist, based on the rapidly rising upstrokes of putative intracellular coupling potentials [fast prepotentials or spikelets, (4, 5)] during ≈200-Hz ripples *in vitro* in low-calcium media that blocked chemical synapses (6). Schmitz and colleagues (7) provided electrophysiological and dye coupling evidence for axoaxonic gap junctions in CA1 and CA3 pyramidal cells as well as in dentate granule cells. Subsequently, both modeling and *in vitro* experimental data suggested that axonal gap junctions could account for very fast oscillations (>70 Hz), including ≈200-Hz ripples (8, 9) as well as play a critical role in the generation of persistent γ (30–70 Hz) (10) and neocortical $\beta 2$ (20–30 Hz) oscillations (11). However, definitive ultrastructural evidence for gap junctions in cortical principal cells has been elusive. Although gap junctions have been reported in freeze–fractured cortical principal neurons (12, 13), reevaluation of the freeze–fracture electron micrographs of those gap junctions based on additional ultrastructural criteria suggested that most were located on glia instead of neurons (14, 15).

Gap junctions are membrane proteins that provide low-resistance pathways for direct electrical and chemical communication between cells. Four candidate gap junction-forming proteins [connexin36 (Cx36), connexin45 (Cx45), connexin50 (Cx50), and connexin57 (Cx57)] and two additional pore-forming proteins [pannexin1 (Px1) and pannexin2 (Px2)] have been identified in central nervous system neurons (16–21). To date, Cx36 is the only gap junction-forming protein documented in cortical GABAergic neurons, as established by ultrastructural methods (22). Cx45 was shown to be abundantly expressed in subsets of cortical neurons in the hippocampus, entorhinal, and occipital cortex by using the LacZ/Cx45 reporter gene expression pattern (18). Px1 and Px2 expression have been shown in hippocampal principal neurons and other cortical neurons by immunohistochemistry; however, it is not clear whether Px1 alone or in combination with Px2 can form functional gap junctions in neurons (23, 24).

In this study, we used thin-section transmission electron microscopy (TEM) to examine large areas (on the order of 10,000 μm^2 of MF axonal membranes) of stratum lucidum under high magnification (×20,000–30,000) to find axonal gap junctions. We also used confocal grid-mapped freeze–fracture replica immunogold labeling (FRIL) (25–27) to find gap junctions on MF axons and to determine the site of gap junctions in reference to hippocampal laminar structure. Thin-section TEM results have been previously reported as an abstract.[§§]

Results

Detection of Axoaxonic Gap Junctions by Thin-Section TEM. We found 10 examples of close appositions/presumptive gap junctions between the unmyelinated MF axons within the MF bundles

Author contributions: F.H.-S., P.R.H., J.E.R., and R.D.T. designed research; F.H.-S., N.K., W.G.M.J., T.Y., K.G.V.D., and J.E.R. performed research; F.H.-S., N.K., W.G.M.J., P.R.H., S.L.W., M.G.S., S.R.Y., M.A.W., J.E.R., and R.D.T. analyzed data; and F.H.-S., J.E.R., and R.D.T. wrote the paper.

The authors declare no conflict of interest.

Freely available online through the PNAS open access option.

Abbreviations: Cx36, connexin36; Cx45, connexin45; Cx50, connexin50; Cx57, connexin57; FRIL, freeze–fracture replica immunogold labeling; MF, mossy fiber; mfb, MF bundle; Px1, pannexin1; Px2, pannexin2; SPB, Sørensen's phosphate buffer; TEM, transmission electron microscopy; ZO, zonula occludens; ZONAB, zonula occludens nucleic acid-binding protein.

†To whom correspondence should be addressed. E-mail: fh81@alumni-mail.gs.columbia.edu.

§Present address: Division of Cerebral Structure, National Institute of Physiological Sciences, Myodaiji, Okazaki 444-8787, Japan.

§§Hamzei-Sichani, F., Janssen, W. G., Hof, P. R., Wearne, S. L., Stewart, M. G., Whittington, M. A., Traub, R. D. (2006) *Gap Junctions Couple Hippocampal Mossy Fiber Axons to Each Other and to CA3 Pyramidal Cell Dendrites* in *Soc. Neurosci Abstr* 132.9/C52.

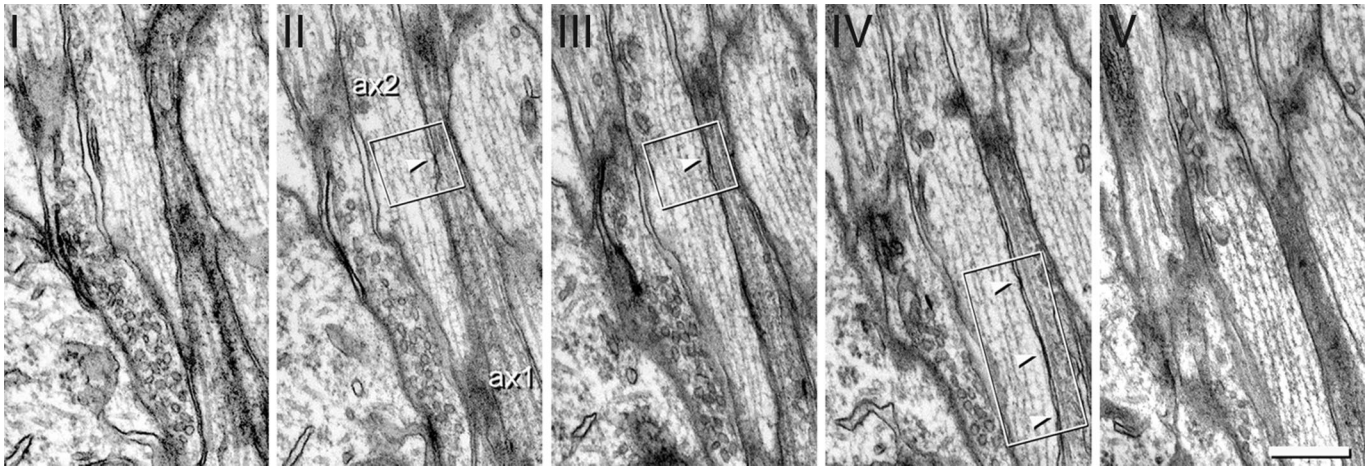

Fig. 1. Electron micrographs of a series of five 50-nm-thick sections cut through a bundle of MF axons in CA3 stratum lucidum of a 4-month-old rat. A total of six presumptive gap junctions between two axons (ax1 and ax2) are marked by arrowheads inside boxed areas in II, III, and IV (the middle arrowhead in IV marks two gap junctions). All putative gap junctions (boxed areas) are shown at higher magnification in Fig. 2. (Scale bar: 300 nm.)

(mfb) in the CA3b stratum lucidum of the ventral rat hippocampus, of which six are illustrated in this paper. In a series of 100 ultrathin sections from the stratum lucidum, we found axoaxonic close appositions that were aggregated along a row and in adjacent 50-nm-thick sections in six instances (Figs. 1 and 2). All these presumptive gap junctions coupled the same pair of axons. Fig. 1 shows a series of five consecutive electron micrographs containing such appositions. Two of the putative gap junctions were derived from separate ultrathin sections (Figs. 1 II and III and 2 *C–F*), and the other four were found in an adjacent section (Figs. 1IV and 2*B*).

These close membrane appositions ranged in length from 30 to 70 nm (mean 45 nm). When the appositions were aggregated in one ultrathin section (Figs. 1IV and 2*B*), the longitudinal

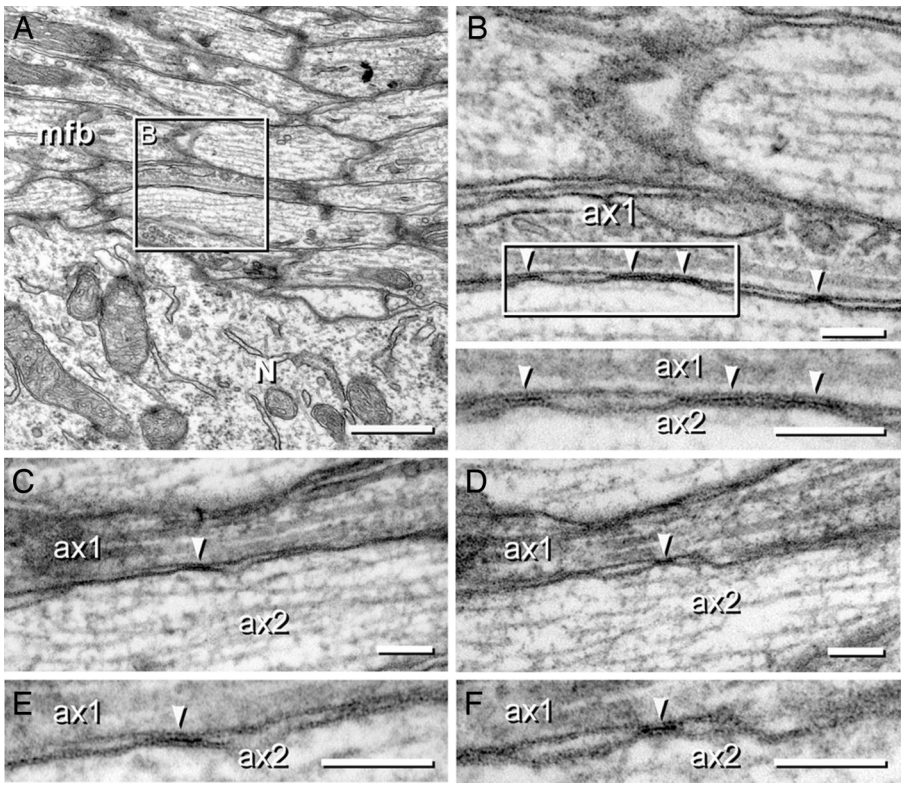

Fig. 2. Electron micrographs of six closely spaced gap junctions between two MF axons, cut longitudinally in CA3 stratum lucidum, corresponding to the gap junctions marked by arrowheads in Fig. 1 II–IV. (*A*) Low-magnification electron micrograph of stratum lucidum showing bundle of MF axons (mfb). N, CA3 pyramidal neuron cell body. (*B*) High-magnification electron micrograph of the region within the box marked in *A*; the arrowheads mark gap junctions between two axons, ax1 and ax2. Higher-magnification electron micrograph of the three gap junctions within the box is shown as an *Inset*. (*C* and *D*) Electron micrographs of two sections (50 nm thick) adjacent to the section shown in *B*, with two additional presumptive gap junctions between the same pair of axons. Arrowheads mark the site of each gap junction between the two axons, ax1 and ax2. These two gap junctions correspond to those seen in Fig. 1 II and III. (*E* and *F*) Higher-magnification electron micrographs of the gap junctions shown in *C* and *D*. [Scale bars: 500 nm (*A*) and 100 nm (*B–F*).]

separation between consecutive close appositions ranged from 35 to 188 nm (mean 115 nm) excluding the two proposed gap junctions that were almost continuous with each other (Fig. 2*B Inset*). Because the close appositions in this sample were all <70 nm in length (and presumably were even thinner perpendicular to the longitudinal axis of the axons), we were not able to capture any particular close apposition in more than one 50-nm-thick section. Putative gap junctions appeared to be isolated in the other four instances.

None of the presumptive axonal gap junctions observed in thin sections had associated submembrane densities. At the site of proposed gap junctions, the axon plasma membranes showed a pentalaminar configuration (Fig. 2 *B–F*). Moreover, a distinct 10-nm periodicity was observed in the extracellular space (Fig. 2*B inset*, middle arrowhead), reminiscent of classic gap junction ultrastructure. However, a central light band, characteristic of heptalaminar gap junctions could not be visualized. Instead, in all cases, the observed close appositions showed a central dark band.

Detection of Axonal Gap Junction by FRIL. Using FRIL, we found a definitive gap junction on a MF axon that was surrounded by other MF axons (numbers 1–4 in Fig. 3*A* and 1–6 in Fig. 3*C*). Confocal laser scanning microscopy images of the replicated tissue localized the bundle of MF axons in the CA3c stratum lucidum. Another gap junction was found on a nearby dendrite (Fig. 3*A*, white arrow). The axonal gap junction formed a small plaque with ≈100 particles (connexons) and was labeled with eight gold bead-conjugated antibodies against Cx36 [Fig. 3*B*; six 18-nm gold beads and two 6-nm gold beads (arrowheads)]. Stereoscopic imaging confirmed the presence of gold beads on the tissue side and only in direct association with the two ultrastructurally identified gap junctions (Fig. 3*B*), therefore reflecting high-resolution labeling of proteins that remain strongly adsorbed to the replica after sodium dodecyl sulfate detergent (SDS) washing (28). The identity of the neuronal process participating in the gap junction with axon 1 (Fig. 3 *A* and *C*) could not be positively determined because of its small size and lack of definitive markers. However, based on the location of the gap junction within a bundle of axons, the unidentified process may be either an additional MF axon or a spine from a nearby dendrite (Fig. 3 *A* and *C*).

Discussion

Thin-section TEM of the stratum lucidum of the adult rat hippocampus revealed that gap junctions are present between dentate granule cell axons and by FRIL, one immunogold-labeled gap junction was found on granule cell axons. The gap junction found by FRIL was internally confirmed to be Cx36-positive based on immunogold labeling by two different sizes of gold beads conjugated to different secondary antibodies. In support, Cx36 is known to form gap junctions between cortical GABAergic interneuron dendrites (22). We also showed thin-section electron micrographs consistent with the presence of gap junctions between identified MF axons. The average size of the gap junctions found in thin sections (45 nm) was similar to the size of the single gap junction found by FRIL (≈50 × 100 nm). The small size of these gap junctions and their apparent low density in the mammalian central nervous system are probably the major sources of difficulty in their detection by using thin-section TEM. Considering the increasing evidence for multiple connexins and multiple morphological types of gap junctions in diverse cell types (15, 29), our data do not exclude the possibility that axonal gap junctions in dentate granule neurons and other cortical principal neurons contain additional as yet unidentified connexins. Pannexins have also been suggested as a component of putative axonal gap junctions (30). However, it is possible that pannexins serve a different role than gap junction coupling in the hippocampus (31).

Further studies are needed to determine the density of MF axonal gap junctions in the stratum lucidum and the subcellular sites to which neuronally expressed connexins are targeted (see Fig. 4 for schematic representation of potential sites for gap junctional coupling between principal neurons of the hippocampus). For example, gap junctions in hippocampal principal neurons may also be localized at dendrites, dendritic spines and giant MF terminals [making MF-CA3 synapses mixed chemical and electrotonic synapses (F.H.-S., W.G.M.J., S.L.W., P.R.H., J.E.R., and R.D.T., unpublished work)].

Physiological Significance of Axoaxonic Gap Junctions. In intracellular recordings from dentate granule neurons in media that blocked chemical synaptic transmission, fast prepotentials (or spikelets), often followed stimulation of the MFs (13). At times, the threshold for eliciting a spikelet in a granule neuron was lower than the threshold for eliciting an antidromic spike in that same cell, suggesting that the spikelet represented a coupling potential caused by a spike in a second, electrically coupled neuron (13). Electrical coupling between MF axons might explain such an observation, if the weaker stimulus evoked a spike in an axon that was electrically coupled to the axon of the recorded neuron and if that spike could cross from axon to axon. We suggest that under physiological conditions, gap junctions between MF axons may also play an important role in amplification of the effects of firing in single dentate granule neurons by allowing the spread of action potentials from axon to axon. We predict that if gap junctions can be eliminated from the hippocampal MF axons in a knockout mouse, then the dentate gyrus in such animals would not exhibit very high-frequency oscillations in media with elevated external K^+ ion concentration and decreased external Ca^{2+} ion concentration. Interestingly, very fast oscillations were unaffected in mice lacking Cx36 (32, 33), suggesting that gap junction proteins in addition to Cx36 may contribute to the formation of axoaxonic gap junctions. On the other hand, another study has reported a decreased incidence of *in vitro* high-frequency ripples in a Cx36 knockout mouse (34).

The role of axonal gap junctions has been investigated in relation to physiological and possibly pathological alterations of electrical activities of the brain, including $\beta 2$ oscillations (20–30 Hz), γ oscillations (30–70 Hz), and very fast oscillations (>100 Hz) (6–11, 35). Oscillations at 250–300 Hz have been recorded in sclerotic human hippocampus, surgically removed and studied *in vitro* (36). Therefore, it is possible that fast oscillatory activity in *in vitro* dentate gyrus under conditions of altered extracellular ion concentrations is relevant to epileptogenesis in some human epileptic patients. The morphological substrates of such oscillations, such as the axoaxonic gap junctions illustrated here, may therefore be a critical disease-influencing parameter.

Morphological Evaluation of Axoaxonic Gap Junctions. Many neuronal gap junctions are known to have associated submembrane densities (37, 38), and the presence of these densities has often been used as a criterion for distinguishing gap junctions from nonspecific and labile membrane appositions (39). Although the definitive molecular identity of these submembrane densities has not been determined, it has been reported that cytoplasmic accessory proteins such as zonula occludens-1 (ZO-1), ZO-2, ZONAB (zonula occludens nucleic acid binding protein) and possibly related members of the membrane-associated guanylate kinase (MAGUK) family of scaffolding proteins may bind and regulate at least some neuronal gap junctions (40). Cx36 and ZO-1 were found to colocalize in 52% of ultrastructurally identified gap junctions in the retina (26, 41). A second group of neuronal gap junctions (25%) of both small and large "plaque-type" were immunogold-labeled with Cx36 but not ZO-1. A third

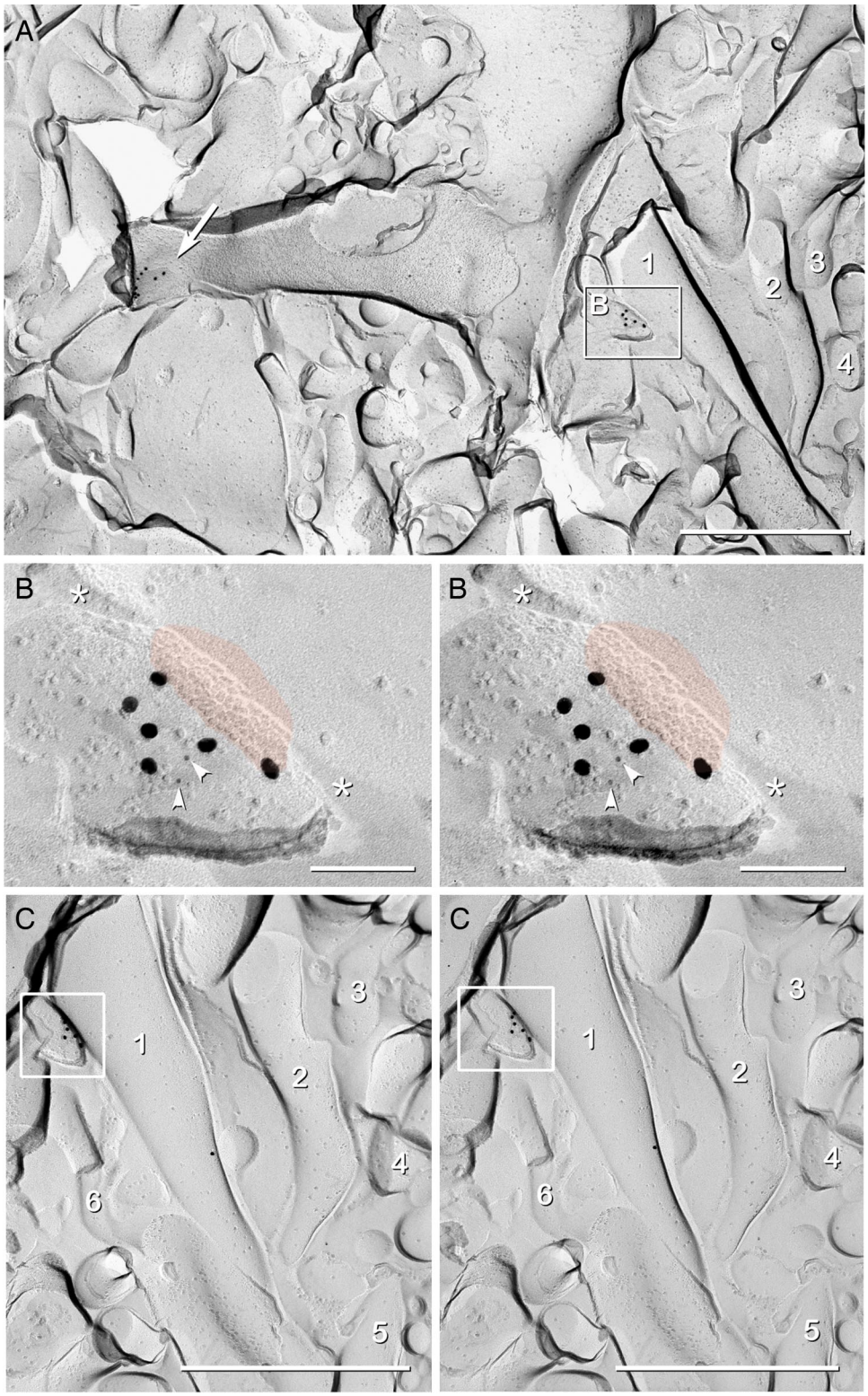

Fig. 3. FRIL electron micrographs of a small-diameter plaque gap junction on a MF axon in the CA3c stratum lucidum of a 150-g rat, labeled with anti-Cx36 immunogold beads. (*A*) Low-magnification FRIL electron micrograph of the axonal gap junction (Box B). Numbers 1–4 represent MF axons in the stratum lucidum of the CA3c field of the rat dorsal hippocampus. The white arrow points to a dendritic gap junction labeled with anti-Cx36 immunogold beads. (*B*) High-magnification stereoscopic electron micrographs of the plaque gap junction (red overlay), which consisted of ≈100 connexons labeled by six 18-nm gold beads and two 6-nm gold beads (arrowheads). Slightly displaced gold beads reflect the length of the double antibody bridge, slight clumping of immunogold, as well as the displacement of lipids and proteins during SDS washing (47). Asterisks mark the extracellular space, which narrows to ≈3 nm at the gap junction contact point. Axon E-face has few intramembrane particles, whereas the P-face of the unidentified but coupled cell process contains densely packed particles around the gap junction. (*C*) High-magnification stereoscopic electron micrographs of the bundle of MF axons (numbers 1–6) tilted ≈45° with respect to the plane shown in *A* to show a clearer view of the interior of axon #1. The area inscribed by the box contains the steeply tilted axonal gap junction. [Scale bars: 1,000 nm (*A* and *C*) and 100 nm (*B*).]

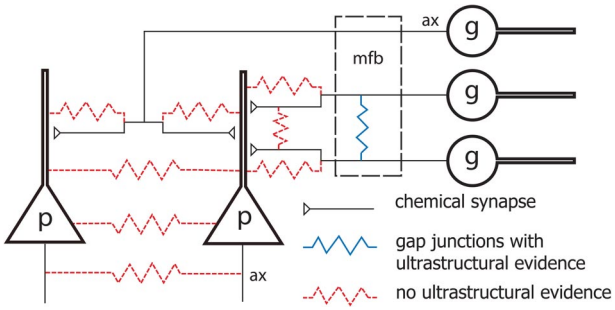

Fig. 4. Schematic drawing of two types of hippocampal principal neurons and potential sites for gap junctional coupling. No ultrastructural evidence exists for the proposed axoaxonic gap junctions between CA3 pyramidal neurons (also true for CA1 and neocortical pyramidal neurons). In this study, we provided ultrastructural evidence for axoaxonic gap junctions in dentate granule neurons (Figs. 1 and 2) and also definitive ultrastructural evidence for the existence of Cx36-immunopositive gap junctions in the axons of the dentate gyrus principal (excitatory) neurons (Fig. 3). Gap junctions between somata or dendrites of cortical principal neurons have not been definitively shown despite several published studies (see p. 279 in ref. 14). MF-CA3 synapses may be mixed (chemical and electrical) synapses, at least in some instances (F.H.-S., W.G.M.J., S.L.W., P.R.H., J.E.R., and R.D.T., unpublished work). p, CA3 pyramidal neuron; g, dentate granule neuron; ax, axon; mfb, mossy fiber bundle.

population of gap junctions (23%) of the small or medium-sized plaque-type gap junctions were immunogold-labeled with ZO-1 but not Cx36. Therefore, the axoaxonic gap junctions found in our thin-section TEM may correspond to the type not commonly associated with scaffolding proteins.

The pentalaminar structure of gap junctions reported in this study had features associated with gap junctions (39). Of greater concern was the possible similarity of these gap junctions to "labile appositions" (see figure 32 in ref. 39). Brightman and Reese (39) found labile pentalaminar junctions between a variety of neuronal processes under certain conditions of fixation and tissue preparation but not under other conditions. Labile pentalaminar junctions were particularly numerous when fixation was poor (marked by swollen processes or dilated endoplasmic reticulum) and, reportedly, when acetone was used as a dehydrating agent. However, labile appositions were very rare in brains treated with osmium tetroxide and *en bloc* aqueous uranyl acetate, as was done in our study (see *Materials and Methods*). The observed pentalaminar structure may be due to intense staining of outer membrane leaflets with heavy metals (uranyl acetate and lead citrate). Artifactual membrane appositions due to improper fixation are usually seen in multiple instances and various parts of the tissue. The gap junctions found by thin-section TEM in our study were in fact rare findings (on average, one gap junction per $\approx$10,000 μm^2 of axonal membranes scanned at high magnification) and are therefore unlikely to be artifacts, a conclusion that is supported by FRIL detection of one Cx36-labeled gap junction on a dentate granule cell axon. Thus, we propose that axoaxonic gap junctions are present at an average density of only a few per axon, as predicted by our model (9), contribute to normal axonal electrical activity *in vivo*, and represent an additional neuronal element that may be involved in altered electrical activity in epilepsy.

Materials and Methods

All animals used in this study were treated under the protocols approved by the Institutional Animal Care and Use Committees of the Mount Sinai School of Medicine and Colorado State University, and all experiments were conducted according to *Principles of Laboratory Animal Care* (U.S. National Institutes of Health Publication No. 86-23, Rev. 2002).

Preparation of Tissues for Thin-Section TEM. Three adult Sprague–Dawley rats (two aged 6 months, one aged 4 months) were deeply anesthetized with an i.p. injection of 30% chloral hydrate (0.3–0.5 ml) and perfused via the ascending aorta with a fixative containing 2.5% formaldehyde (prepared from paraformaldehyde), 3% glutaraldehyde, 2 mM $CaCl_2$, 4 mM $MgSO_4$, and 0.1 M sodium cacodylate buffer (pH 7.25) at 38°C. Perfusion was set at a flow rate of 45 ml/min supported by a peristaltic pump for 15 min. After 2 h at room temperature, the embalmed rat was transferred to a cold room and kept overnight at 4°C. The brain was dissected and sliced at 600-μm thickness in the horizontal plane in chilled 0.15 M PBS by using a VT1000 vibrating blade microtome (Leica Microsystems, Bannockburn, IL). The CA3 region was cut from six brain slices, washed with chilled PBS for 3×10 min each and transferred to 2% OsO_4 in PBS (4°C) for 2 h in the dark. Slices were washed in sodium acetate buffer and stained *en bloc* with aqueous 2% uranyl acetate at 10°C for 2 h in the dark. After washing in PBS, tissue was dehydrated in ascending concentrations of ethanol at room temperature, followed by propylene oxide and impregnated with 50/50 Araldite-Epon (Embed-812)/propylene oxide (Araldite 502/EMbed 812 kit, Electron Microscopy Sciences, Hatfield, PA) overnight and then with fresh Araldite-Epon mixture for 6 h. Slices were transferred to capsules filled with Araldite-Epon mixture and kept at 60°C for 48 h under partial vacuum (20–25 mm Hg). Blocks were trimmed to a trapezoid containing the CA3 stratum lucidum by using a cryotrim 45 diamond knife (DiATOME, Hatfield, PA) on an Ultracut E ultramicrotome (Reichert–Jung, Nussloch, Germany). A series of 100 ultrathin sections ($\approx$50 nm in thickness) were cut by using a diamond knife (Delaware Diamond Knives, Wilmington, DE), mounted on Formvar-coated slot grids (Electron Microscopy Sciences), and stained for 45 min with 1% uranyl acetate and 3 min with Reynolds' lead citrate (42). Detailed methods for tissue preparation are described (42). Thin sections were photographed by using a $2{,}000 \times 2{,}000$ Advantage CCD camera (Advanced Microscopy Techniques, Danvers, MA) at 80 kV on a 1200EX electron microscope (JEOL, Peabody, MA). All electron microscopy reagents were from Sigma–Aldrich (St. Louis, MO) unless stated otherwise.

Freeze–Fracture and Immunogold Labeling. A 150-g Sprague–Dawley rat was deeply anesthetized for 3–5 min after i.p. injections of ketamine and xylazine (120–160 mg/kg and 12–16 mg/kg, respectively) and fixed by whole-body vascular perfusion with 4% formaldehyde in Sørensen's phosphate buffer (SPB), a 1:5 mixture of 0.15 M NaH_2PO_4 and 0.15 M Na_2HPO_4 (pH 7.4) containing 0.05% sodium azide. Coronal brain slices were cut at 100-μm thickness by using a refrigerated Lancer Vibratome 3000 (Technical Products International, St. Louis, MO) that maintained the samples at 4°C. Hippocampal slices were infiltrated with 30% glycerol, mounted on aluminum "Slammer" supports (43), and frozen by contact with a liquid nitrogen-cooled metal mirror (Ultra-Freeze MF7000; RMC Products, Tucson, AZ). Frozen samples were fractured and replicated in a JEOL/RMC 9010C freeze–fracture device, then bonded to gold "index" grids (Electron Microscopy Sciences) by using 1.5–2% Lexan (GE Plastics, Pittsfield, MA) dissolved in ethylene dichloride, according to our published procedures (26, 27, 44). The Lexan-stabilized samples were thawed and photomapped with a LSM510 Meta laser scanning confocal microscope (Carl Zeiss MicroImaging, Thornwood, NY) by using tissue autofluorescence.

Replicas were washed in 2.5% SDS detergent in 0.16% Tris·HCl buffer (pH 8.9) with constant stirring for 29 h at 48.5°C. After the initial 4 h in the SDS solution, the sample was digested for 1.25 h in 4% collagenase D (Roche Applied Science, Indianapolis, IN) in 0.15 M SPB, followed by an additional 18–24 h in SDS solution. The replica was rinsed in blocking buffer (45) consisting of 10% heat-inactivated goat serum plus

1.5% fish gelatin in SPB (pH 7.4) and labeled for 140 min by using rabbit polyclonal anti-Cx36 (Ab36–4600, Invitrogen/Zymed, Carlsbad, CA) and mouse monoclonal anti-Cx32 antibodies (MAB 3069; Chemicon International, Temecula, CA) diluted to 10 μg/ml in blocking buffer (46). Samples were rinsed and counterlabeled for 17 h by using goat anti-rabbit IgG conjugated to 6 nm and 18 nm gold beads (Jackson ImmunoResearch, West Grove, PA) and goat anti-mouse IgG conjugated to 12-nm gold beads (Jackson ImmunoResearch). Before electron microscopic examination, the samples were coated with 20 nm of carbon on the labeled side (to immobilize gold beads and to create a barrier to prevent reattachment of displaced gold beads during subsequent removal of the Lexan support film), and the Lexan support film was removed by immersing the grids in 60°C ethylene dichloride solvent for 6–8 h.

Replicas were examined at 100 kV on JEOL 2000 EX-II and JEOL 1200 EX TEMs. Stereoscopic electron micrographs obtained with an 8° included angle were used for assessing complex three-dimensional membrane topography as well as for confirming that each immunogold bead was on the tissue side of the replica (27) and for discriminating the smaller (6 nm) gold beads from the similarly electron-opaque granularity of the platinum replica (25, 26). Freeze–fractured neuronal processes were identified according to established criteria (14).

Image Processing of FRIL Electron Micrographs. FRIL electron micrograph negatives were digitized by an ArtixScan 2500f digital scanner (Microtek, Carson, CA) and processed by using Adobe Photoshop CS2 (Adobe Systems, San Jose, CA), with "levels" used for maximal contrast expansion and "brightness/contrast" used to optimize image contrast and definition.

We thank Profs. Takaichi Fukuda, Rodolfo Llinás, and Constantino Sotelo for helpful discussions and encouragement. This work is dedicated to the memory of Eberhard H. Buhl and Mircea Steriade. This work was supported by the Medical Research Council (U.K.), the Wellcome Trust, and National Institute of Neurological Disorders and Stroke/National Institutes of Health Grants 5R01NS044133-04 and 5R01NS046058-04.

1. Henze DA, Urban NN, Barrionuevo G (2000) *Neuroscience* 98:407–427.
2. Jung MW, McNaughton BL (1993) *Hippocampus* 3:165–182.
3. Henze DA, Wittner L, Buzsáki G (2002) *Nat Neurosci* 5:790–795.
4. Valiante TA, Perez Velazquez JL, Jahromi SS, Carlen PL (1995) *J Neurosci* 15:6946–6956.
5. Spencer WA, Kandel ER (1961) *J Neurophysiol* 24:272–285.
6. Draguhn A, Traub RD, Schmitz D, Jefferys JG (1998) *Nature* 394:189–192.
7. Schmitz D, Schuchmann S, Fisahn A, Draguhn A, Buhl EH, Petrasch-Parwez E, Dermietzel R, Heinemann U, Traub RD (2001) *Neuron* 31:831–840.
8. Traub RD, Bibbig A (2000) *J Neurosci* 20:2086–2093.
9. Traub RD, Schmitz D, Jefferys JG, Draguhn A (1999) *Neuroscience* 92:407–426.
10. Traub RD, Cunningham MO, Gloveli T, LeBeau FE, Bibbig A, Buhl EH, Whittington MA (2003) *Proc Natl Acad Sci USA* 100:11047–11052.
11. Roopun AK, Middleton SJ, Cunningham MO, LeBeau FE, Bibbig A, Whittington MA, Traub RD (2006) *Proc Natl Acad Sci USA* 103:15646–15650.
12. Schmalbruch H, Jahnsen H (1981) *Brain Res* 217:175–178.
13. MacVicar BA, Dudek FE (1982) *J Neurophysiol* 47:579–592.
14. Rash JE, Duffy HS, Dudek FE, Bilhartz BL, Whalen LR, Yasumura T (1997) *J Comp Neurol* 388:265–292.
15. Nagy JI, Dudek FE, Rash JE (2004) *Brain Res Rev* 47:191–215.
16. Condorelli DF, Belluardo N, Trovato-Salinaro A, Mudo G (2000) *Brain Res Rev* 32:72–85.
17. Hombach S, Janssen-Bienhold U, Sohl G, Schubert T, Bussow H, Ott T, Weiler R, Willecke K (2004) *Eur J Neurosci* 19:2633–2640.
18. Maxeiner S, Kruger O, Schilling K, Traub O, Urschel S, Willecke K (2003) *Neuroscience* 119:689–700.
19. Rash JE, Davidson KG, Kamasawa N, Yasumura T, Kamasawa M, Zhang C, Michaels R, Restrepo D, Ottersen OP, Olson CO, *et al.* (2005) *J Neurocytol* 34:307–341.
20. Rash JE, Yasumura T, Dudek FE, Nagy JI (2001) *J Neurosci* 21:1983–2000.
21. O'Brien JJ, Li W, Pan F, Keung J, O'Brien J, Massey SC (2006) *J Neurosci* 26:11624–11636.
22. Fukuda T, Kosaka T, Singer W, Galuske RA (2006) *J Neurosci* 26:3434–3443.
23. Vogt A, Hormuzdi SG, Monyer H (2005) *Brain Res Mol Brain Res* 141:113–120.
24. Zoidl G, Petrasch-Parwez E, Ray A, Meier C, Bunse S, Habbes HW, Dahl G, Dermietzel R (2007) *Neuroscience* 146:9–16.
25. Pereda A, O'Brien J, Nagy JI, Bukauskas F, Davidson KG, Kamasawa N, Yasumura T, Rash JE (2003) *J Neurosci* 23:7489–7503.
26. Rash JE, Pereda A, Kamasawa N, Furman CS, Yasumura T, Davidson KG, Dudek FE, Olson C, Li X, Nagy JI (2004) *J Neurocytol* 33:131–151.
27. Rash JE, Yasumura T (1999) *Cell Tissue Res* 296:307–321.
28. Fujimoto K (1995) *J Cell Sci* 108:3443–3449.
29. Connors BW, Long MA (2004) *Annu Rev Neurosci* 27:393–418.
30. Bruzzone R, Hormuzdi SG, Barbe MT, Herb A, Monyer H (2003) *Proc Natl Acad Sci USA* 100:13644–13649.
31. Thompson RJ, Zhou N, MacVicar BA (2006) *Science* 312:924–927.
32. Buhl DL, Harris KD, Hormuzdi SG, Monyer H, Buzsáki G (2003) *J Neurosci* 23:1013–1018.
33. Hormuzdi SG, Pais I, LeBeau FE, Towers SK, Rozov A, Buhl EH, Whittington MA, Monyer H (2001) *Neuron* 31:487–495.
34. Maier N, Guldenagel M, Sohl G, Siegmund H, Willecke K, Draguhn A (2002) *J Physiol* 541:521–528.
35. Towers SK, LeBeau FE, Gloveli T, Traub RD, Whittington MA, Buhl EH (2002) *J Neurophysiol* 87:1165–1168.
36. Gabriel S, Njunting M, Pomper JK, Merschhemke M, Sanabria ER, Eilers A, Kivi A, Zeller M, Meencke HJ, Cavalheiro EA, *et al.* (2004) *J Neurosci* 24:10416–10430.
37. Sotelo C (1975) in *Golgi Centennial Symposium: Perspectives in Neurobiology*, ed Santini M (Raven, New York), pp 355–365.
38. Sotelo C, Korn H (1978) *Int Rev Cytol* 55:67–107.
39. Brightman MW, Reese TS (1969) *J Cell Biol* 40:648–677.
40. Ciolofan C, Li XB, Olson C, Kamasawa N, Gebhardt BR, Yasumura T, Morita M, Rash JE, Nagy JI (2006) *Neuroscience* 140:433–451.
41. Li X, Olson C, Lu S, Kamasawa N, Yasumura T, Rash JE, Nagy JI (2004) *Eur J Neurosci* 19:2132–2146.
42. Friedrich VL, Jr, Mugnaini E (1981) in *Neuroanatomical Tract-Tracing Methods*, eds Heimer L, RoBards MJ (Plenum, New York), pp 345–375.
43. Heuser JE, Reese TS, Dennis MJ, Jan Y, Jan L, Evans L (1979) *J Cell Biol* 81:275–300.
44. Rash JE, Dillman R, Morita M, Whalen LR, Guthrie PB, Fay-Guthrie D, Wheeler DW (1995) in *Techniques in Modern Biomedical Microscopy*, eds Shotton DM, Severs NJ (Wiley–Liss, New York), pp 127–150.
45. Dinchuk JE, Johnson TJ, Rash JE (1987) *J Electron Microsc Tech* 7:1–16.
46. Rash JE, Staines WA, Yasumura T, Patel D, Furman CS, Stelmack GL, Nagy JI (2000) *Proc Natl Acad Sci USA* 97:7573–7578.
47. Kamasawa N, Furman CS, Davidson KG, Sampson JA, Magnie AR, Gebhardt BR, Kamasawa M, Yasumura T, Zumbrunnen JR, Pickard GE, *et al.* (2006) *Neuroscience* 142:1093–1117.